Asymmetric regular sampling SPWM method based on tangent approximation algorithm

LI Wei[1]*, LI Weibo*[1,2]*, XU Cong*[1]*, LU Yue*[1]*, CHEN Hui*[1]

1 School of Automation, Wuhan University of Technology, Wuhan 430070, China

2 Institute of Technology, Tibet University, Lasa 850012, China

Abstract: [**Objectives**] In order to improve the quality of sinusoidal waveform output by the ship's high-frequency inverter charging device and reduce the CPU occupancy rate, this paper proposes a sinusoidal pulse width modulation (SPWM) method of asymmetric regular sampling based on tangent approximation. [**Methods**] According to the basic principle and calculation method of the asymmetric regular sampling SPWM method based on tangent approximation, a Matlab/Simulink simulation model is built, and then the software algorithm flow that can be used in the high-frequency inverter charging device is designed together with the actual output of the tangent approximation method. The effects are then compared and verified by experiments. [**Results**] The simulation results show that under pure resistive load and resistive inductive load, the total harmonic distortion (THD) of the load-end waveform based on the tangent approximation method is 2.12% and 2.08%, respectively, and its waveform quality is better than that of symmetric regular sampling. The experimental results show that the THD of a load-end waveform based on the tangent approximation method is significantly lower than that of the symmetric regular sampling method. When the effective value of the input line voltage is 580 V (the modulation ratio is 0.8), the quality of the output waveform is relatively optimal. [**Conclusions**] The asymmetric regular sampling SPWM method based on tangent approximation overcomes the shortcomings of the traditional symmetric regular sampling method, such as the low quality of the output waveform and high sampling frequency and high CPU occupancy rate in the traditional asymmetric regular sampling method. The research results can provide a reference for the design of high-frequency inverter charging devices on ships.

Key words: electric inverter; sinusoidal pulse width modulation; regular sampling; tangent approximation

CLC number：U665.12

0　Introduction

At present, power systems of warships are of increasingly complex structural topology, with gradually increasing quantities and types of equipment. As bridges between power grids and electrical equipment, high-frequency inverters can supply uninterrupted power for warship power systems, thus being an important guarantee of warship survivability and combat capability. With the development of power electronics, sinusoidal pulse width modulation (SPWM) has received more and more attention in the field of inverter control. Specifically, natural sampling and symmetric regular sampling are most widely used. According to its design principle, natural sampling is more suitable for analog circuits, featuring simple circuits, high waveform quality, and fast response. However, the parameters of this method can easily drift. Moreover, pure analog circuits will reduce the integration of controllers and increase the difficulty of subsequent hardware modification. Symmetric regular sampling is a digital-

control-oriented method based on natural sampling, featuring simple principles, easy digitization, high integration of control systems, and convenient optimization in a later stage. However, compared with natural sampling, this method has increased harmonic content and relatively poor waveform quality. Therefore, it is worth studying how to improve symmetric regular sampling to enhance waveform quality, on the premise of avoiding a large amount of computation.

Chen et al. [1] proposed SPWM sampling based on asymmetric rules of intersections. However, compared with symmetric regular sampling, this method has doubled sampling times and a larger amount of computation. On the basis of research results from Reference [1], Wang et al. [2] estimated the switching time of intersection-based sampling, thus producing sine waves close to those in natural sampling. However, the problems of many sampling times and a large amount of computation still remained unsolved. Zhou et al. [3] proposed a method of optimized asymmetric regular sampling. With the principle of similar triangles, this method makes the output waveforms of traditional asymmetric regular sampling closer to sinusoidal waveforms to a certain extent. However, it also requires too many times of sampling.

Therefore, this paper proposed an SPWM method of asymmetric regular sampling based on tangent approximation and carried out simulation analysis and engineering experimental verification. Compared with traditional symmetric regular sampling, this method produces a modulation effect closer to that produced by natural sampling. Moreover, compared with traditional asymmetric regular sampling, this method has a sampling table length cut by about half, thus reducing the demand for memory space.

1 Traditional sampling methods

Fig. 1 shows the basic principles of traditional sampling methods commonly used in engineering, and Table 1 lists relevant parameters. In the figure, A' and B' are the intersections between a sinusoidal modulation wave and a triangular carrier wave. A and B are approximately simulated points of A' and B', respectively. t'_{on} is the high-level time before the sampling point C; t''_{on} is the high-level time after the sampling point C. t'_{off} is the low-level time before the sampling point C after the end of the previous period. t''_{off} is the low-level time after the sampling point C before the start of the next period. In natural sampling (Fig. 1 (a)), the intersections A and B between a sinusoidal modulation wave and a triangular carrier wave correspond to the switching time t_A and t_B of a switching device. In symmetric regular sampling (Fig. 1 (b)), the trough in each period of a triangular carrier wave corresponds to a sine-wave sampling point (point C). Then, a parallel line of the t-axis is made at point C, which intersects the two oblique lines of the triangular carrier wave at points A and B. Thus, the corresponding t_A and t_B are the switching time of a switching tube. Different from symmetric regular sampling, traditional asymmetric regular sampling (Fig. 1 (c)) will sample twice in each period of a triangular carrier wave. Specifically, sampling will be done once at the trough and the crest, respectively, as shown by points C and D in the figure. Parallel lines of the t-axis are made through points D and C respectively, intersecting the two oblique edges of the triangular carrier wave at points A and B. Thus, the corresponding t_A and t_B are the switching time of a switching tube.

According to Fig. 1 (a), the pulse width t_{on1} in natural sampling is given by

(a) Natural sampling   (b) Symmetric regular sampling   (c) Traditional asymmetric regular sampling
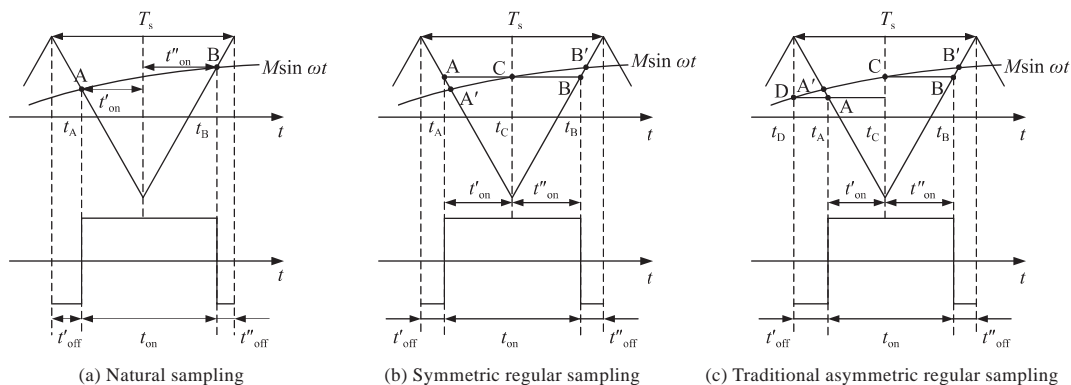
Fig. 1   Schematic diagram of traditional sampling methods

$$t_{on1} = \frac{T_s}{2} \left\{ 1 + \frac{M}{2} [\sin(\omega t_A) + \sin(\omega t_B)] \right\} \quad (1)$$

According to Fig. 1 (b), the pulse width t_{on2} in symmetric regular sampling is given by

$$t_{on2} = \frac{T_s}{2} [1 + M\sin(\omega t_C)] \quad (2)$$

According to Fig. 1 (c), the pulse width t_{on3} in asymmetric regular sampling is given by

$$t_{on3} = \frac{T_s}{2} \left\{ 1 + \frac{M}{2} [\sin(\omega t_C) + \sin(\omega t_D)] \right\} \quad (3)$$

Table 1   Parameters of traditional sampling method

Parameter	Description	Remark
T_s	Sampling period of a triangular carrier wave	Correspond to switching frequency
t_{on}	ON time period of the switch (pulse width)	$t_{on} = t'_{on} + t''_{on}$
t_{off}	OFF time period of the switch	$t_{off} = t'_{off} + t''_{off}$
t_A	ON time of the switch	—
t_B	OFF time of the switch	$t_{on} = t_B - t_A$
t_C, t_D	Sampling time corresponding to sampling points	—
M	Modulation ratio	Ratio of the amplitude of the sinusoidal modulation wave to that of triangular carrier wave
ω	Angular frequency of the sinusoidal modulation wave	—

Table 2 lists the advantages and disadvantages of the three traditional sampling methods. From Table 2, symmetric regular sampling is of ordinary precision, while traditional asymmetric regular sampling needs more computation and doubled sampling frequency. In the field of digital control, the doubling of sampling frequency means that an array space of twice the length of the space in symmetric regular sampling needs to be reserved in the program in order for data storage. This places a high requirement on the storage space of the CPU in the case of higher sampling frequency. Therefore, symmetric regular sampling is generally adopted for digital control in practical engineering applications.

Table 2   Comparison of traditional sampling methods

Sampling method	Advantage	Disadvantage
Natural sampling	High precision	A large amount of computation, inconvenient digital control
Symmetric regular sampling	A relatively small amount of computation, convenient digital control	Ordinary precision
Asymmetric regular sampling	With precision higher than that of symmetric regular sampling, convenient digital control	A relatively large amount of computation, with sampling frequency twice that of symmetric regular sampling

In view of this problem, asymmetric regular sampling based on tangent approximation was proposed in this paper for SPWM. This method only slightly increases the amount of computation, without increasing sampling frequency, and is suitable for engineering practice.

2   Asymmetric regular sampling based on tangent approximation

2.1   Principle of the tangent-approximation-based method

Fig. 2 shows the basic principle of asymmetric regular sampling based on tangent approximation. Sampling is carried out at a trough of a triangular carrier wave. Specifically, a vertical line is made at the trough, intersecting the sine wave at point C. Then, a tangent of the sine wave is made at point C, intersecting oblique edges of the triangular carrier wave at points A and B. Thus, t_A and t_B are the corresponding switching time. In order for convenient analysis, this paper will normalize amplitude y of the triangular wave, namely,

$$\begin{cases} y = -\frac{4}{T_s}(t - kT_s) - 1, & \left(k - \frac{1}{2}\right)T_s \leqslant t \leqslant kT_s \\ y = \frac{4}{T_s}(t - kT_s) - 1, & kT_s < t \leqslant \left(k - \frac{1}{2}\right)T_s \end{cases} \quad (4)$$

where t is sampling time; $k = 0, 1, …, K$ is the number of periods corresponding to the current sampling point, which is a non-negative integer; K is the maximum number of periods.
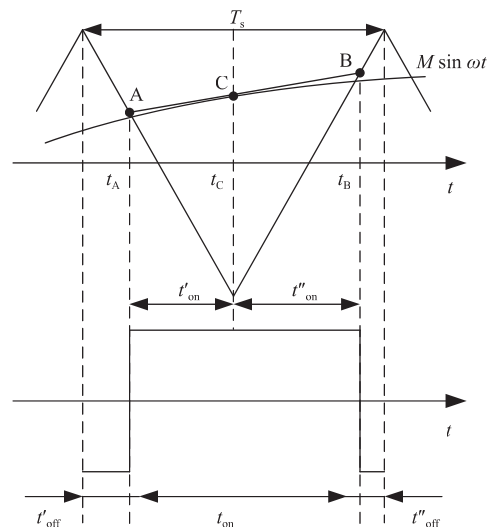
Fig. 2   Schematic diagram of asymmetric regular sampling method based on tangent approximation

The function y_{AB} of the tangent AB can be obtained through the derivation of the modulation-wave function at t_C, which is expressed as follows:

$$y_{AB} = \omega M \cos(\omega k T_s) \times (t - kT_s) + M\sin(\omega k T_s) \quad (5)$$

The switching time t_A and t_B can be calculated by combining Formulas (4) and (5):

$$t_A = \left[k - \frac{M\sin(\omega k T_s) + 1}{\omega M\cos(\omega k T_s) + 4} \right] T_s \quad (6)$$

$$t_B = \left[k - \frac{M\sin(\omega k T_s) + 1}{\omega M\cos(\omega k T_s) - 4} \right] T_s \quad (7)$$

Pulse width t_{on4} in the asymmetric regular sampling based on tangent approximation can be obtained by combining Formulas (6) and (7):

$$t_{on4} = t_B - t_A = \frac{8T_s[1 + M\sin(\omega k T_s)]}{16 - \omega^2 M^2 \cos^2(\omega k T_s)} = \frac{8T_s[1 + M\sin(\omega k T_s)]}{16 - \omega^2 M^2 + \omega^2 M^2 \sin^2(\omega k T_s)} \quad (8)$$

From Formula (8), asymmetric regular sampling based on tangent approximation is different from natural sampling. As k and T_s are both known, it is convenient to solve pulse width t_{on4} by a computer. Compared with symmetric regular sampling and asymmetric regular sampling, asymmetric regular sampling based on tangent approximation has a slightly increased amount of computation. As the cosinoidal component in Formula (8) can be replaced by a sinusoidal one, the sampling table length of asymmetric regular sampling based on tangent approximation can be reduced by half, compared with that of asymmetric regular sampling. In other words, it is consistent with the sampling table length of symmetric regular sampling.

In order for easy implementation of Formula (8) in a single-chip microcomputer, it is necessary to calculate the high-level time (namely, the turn-on time of a switching tube) of each switching period in the program. In this paper, the count value n_{on} corresponding to each pulse width in an SPWM pulse sequence is used in this paper to represent high-level time, namely,

$$n_{on} = \frac{8P[1 + M\sin(2\pi i/N)]}{16 - \omega^2 M^2 + \omega^2 M^2 \sin^2(2\pi i/N)} \quad (9)$$

where P is the timer's count value corresponding to each pulse period; for the sake of safety, the modulation ratio in this paper was set within a range of $M = 0.05 - 0.95$; i is pulse sequence number in the current period; N is the number of triangular carrier waves in each sinusoidal period, that is, the number of pulses in each sinusoidal period.

2.2　Comparison with traditional sampling methods

Fig. 3 shows the comparison of SPWM waveforms generated by tangent approximation, symmetric regular sampling, and natural sampling. In Fig. 3, A_N and B_N are intersections between the sine wave and the triangular wave. Their corresponding time represents the ON and OFF time of a pulse (blue pulse curve) in natural sampling, respectively. A_T and B_T are intersections between the tangent of the sine wave at point C and the triangular wave. Their corresponding time represents the ON and OFF time of the pulse (red pulse curve) in the tangent-approximation-based method, respectively. A and B are intersections between the horizontal line at point C and the triangular wave. Their corresponding time represents the ON and OFF time of the pulse (black pulse curve) in symmetric regular sampling, respectively.
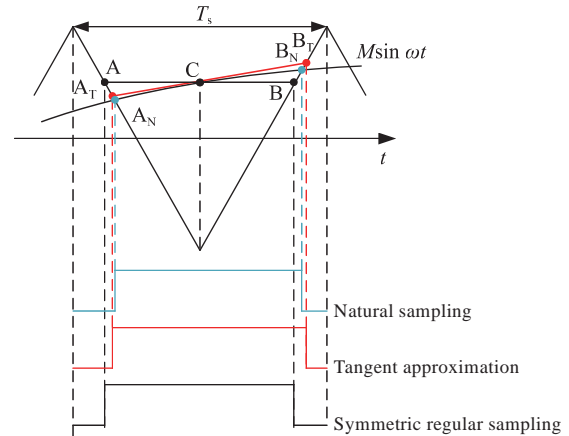
Fig. 3　Comparison chart of the modulation waves

In essence, regular sampling is digitalized processing of natural sampling, aiming to obtain waveforms closer to those in natural sampling. From Fig. 3, whether in terms of overall turn-on time or in terms of pulse ON and OFF time, asymmetric regular sampling based on tangent approximation is obviously closer to natural sampling than symmetric regular sampling does. Thus, waveforms produced by asymmetric regular sampling based on tangent approximation will be closer to actual sine waveforms than those produced by symmetric regular sampling, theoretically.

3　Modeling and simulation analysis

This paper analyzed the tangent-approximation-based SPWM by Matlab/Simulink for verification. Fig. 4 shows the simulation model[4-7], which mainly includes a DC source module, an inverter module, an LC filter module, a load module, and an SPWM module [8-9] of the strong-current part. Key simulation parameters of Fig. 4 are shown in Table 3. Specifically, the inverter module adopts default pa-
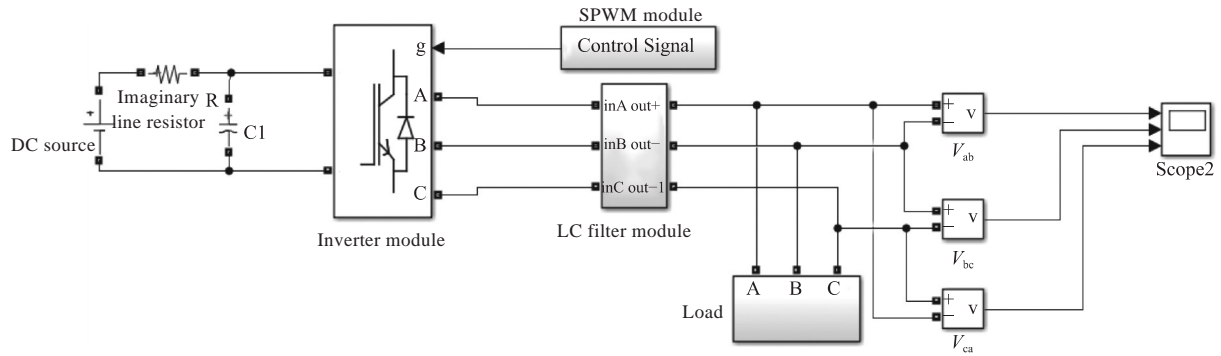
Fig. 4   Simulation model of the experimental device

Table 3   Key parameters of the simulation model

Parameter	Value
DC source voltage/V	1 000
Line resistance/Ω	0.1
DC filter capacitance/μF	1 500
Output filter inductance/mH	5
Output filter capacitance/μF	22
Sinusoidal modulation-wave frequency/Hz	50
Switching frequency/Hz	4 000
Modulation ratio	1

rameters from the simulation platform.

The SPWM module consists of a sinusoidal modulation module, an S-function module, and a PWM generator module (Fig. 5). Specifically, the sinusoidal modulation module functions to generate a sine wave of desired frequency (with an amplitude of 1). The S-function module and the PWM generator module function to form pulse width according to sinusoidally-changed SPWM waves. Symmetric regular sampling and asymmetric regular sampling based on tangent approximation can be randomly switched by changing internal programs of the S-function module.

Fig. 6 shows simulated waveforms obtained by asymmetric regular sampling based on tangent approximation. Specifically, Fig. 6 (a) shows the sinusoidal modulation wave, the output PWM duty ratio, and the SPWM signal; Fig. 6 (b) shows the obtained load-end three-phase line voltages (V_{ab}, V_{bc}, and V_{ca}). For convenient comparison, the amplitudes of both the sinusoidal modulation wave and the SPWM switch signal are normalized in this paper. From Fig. 6 (a), the output PWM duty ratio and the SPWM signal change consistently with the sinusoidal modulation wave. From Fig. 6 (b), after LC filtering, three-phase line voltages at the load end are of standard sinusoidal waveforms, thus verifying the feasibility of asymmetric regular sampling SPWM based on tangent approximation.

In order to further analyze the advantages of the tangent-approximation-based method, without changing parameters of strong-current modules, sinusoidal modulation frequency, and switching frequency, we changed the internal programs of the S-function module. On this basis, load-end waveforms from the tangent-approximation-based method and symmetric regular sampling were comparatively simulated in terms of fast Fourier transform
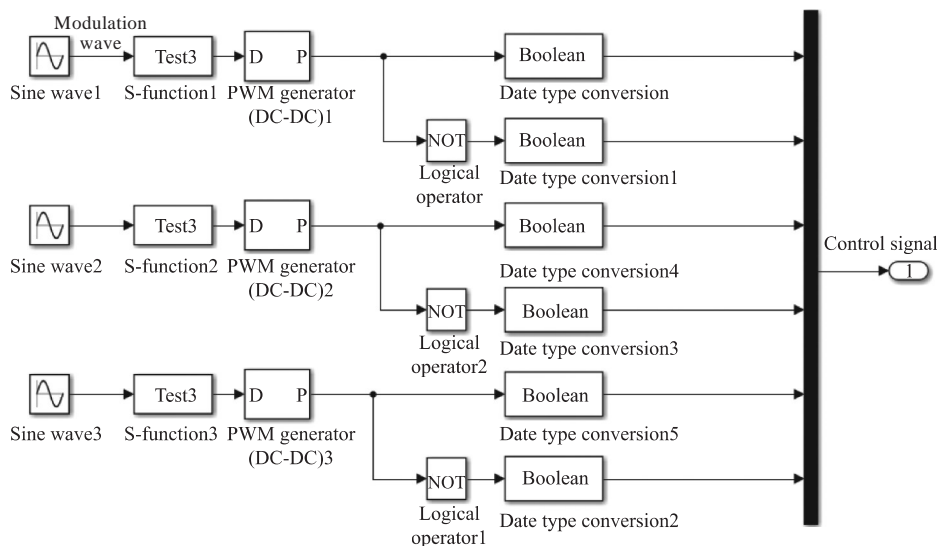
Fig. 5   Simulation model of SPWM module
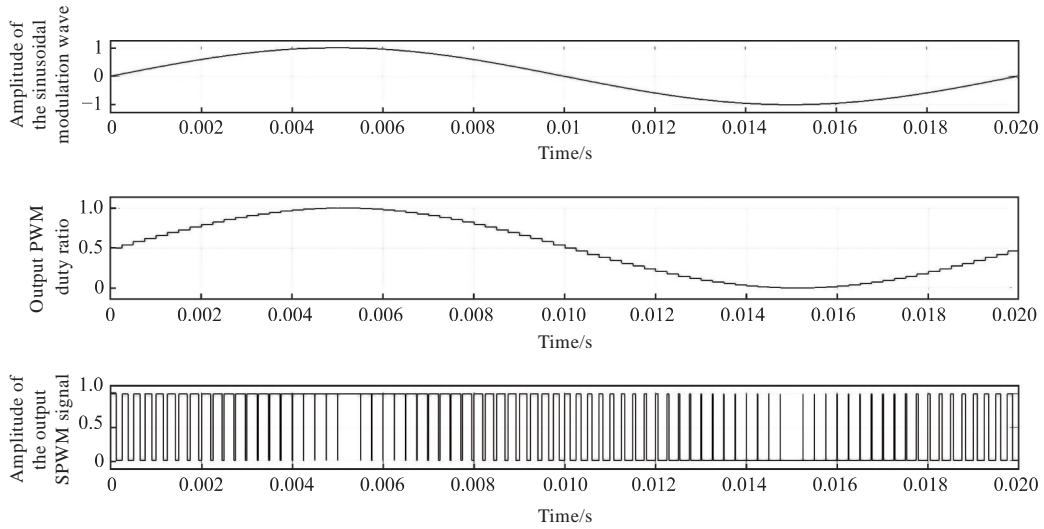
(a) Sinusoidal modulation wave, output PWM duty ratio, and SPWM signal
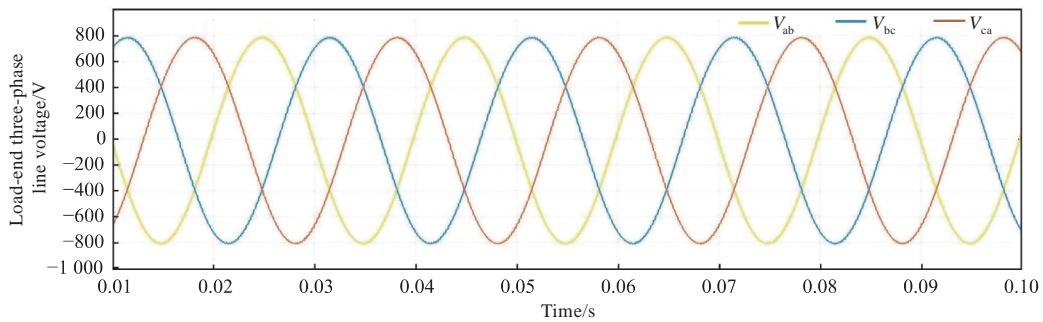
(b) Waveforms of the load-end three-phase line voltages

Fig. 6   Simulation waveform of tangent approximation

(FFT) (Fig. 7) [10-12]. In order to guarantee the strictness of analysis results, this paper took a resistive load (100 Ω) and a resistive-inductive load (100 Ω,

0.2 H) for simulation.

For example in Fig. 7 (a), Fundamental (50 Hz) = 998.2, which indicates fundamental amplitude with

(a) Tangent approximation (Pure resistive load)

(b) Symmetric regular sampling (Pure resistive load)

(c) Tangent approximation (Resistive-inductive load)

(d) Symmetric regular sampling (Resistive-inductive load)
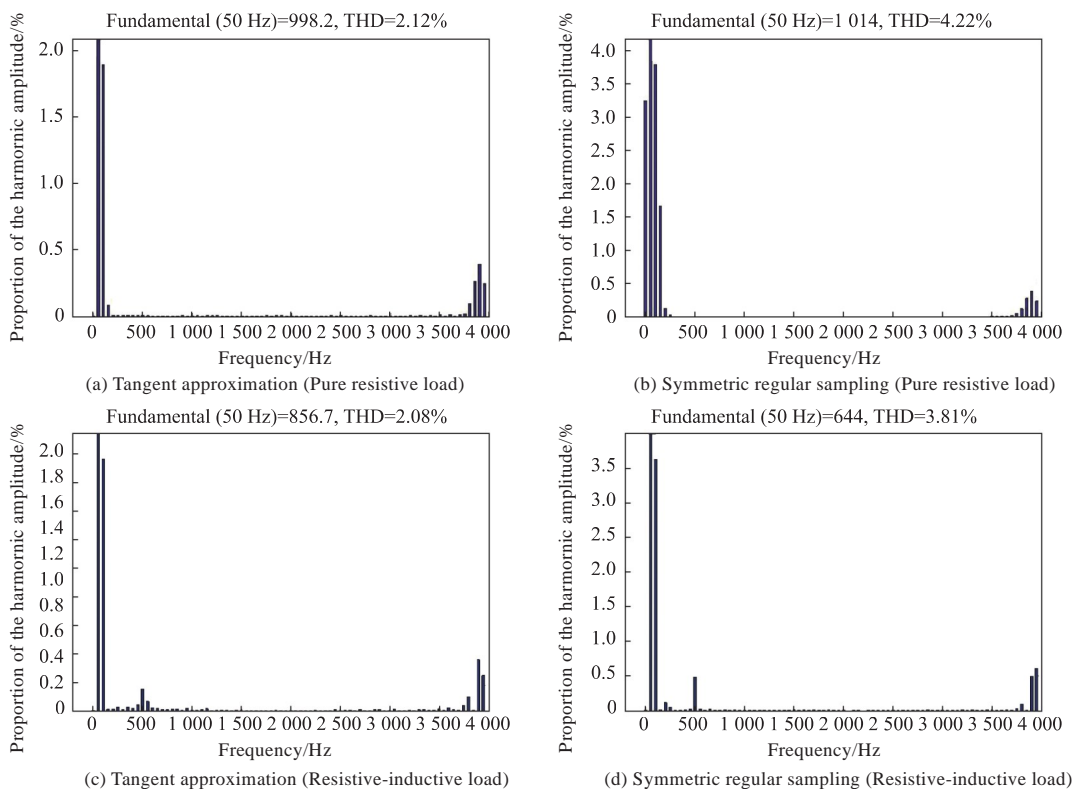
Fig. 7   FFT analysis results

a frequency of 50 Hz. Due to different algorithms or loads, in the same duty ratio, the fundamental amplitude is also different, as shown in Figs. 7 (a)-7(d). The ordinates in Fig. 7 refer to the proportions of the harmonic amplitude at various frequencies in fundamental amplitude, from which total harmonic distortion (THD) can be calculated. From Fig. 7, under a pure resistive load, the THD of a load-end waveform based on tangent approximation is 2.12%, while that of a load-end waveform based on symmetric regular sampling is 4.22%. Under a resistive-inductive load, the THD of a load-end waveform based on tangent approximation is 2.08%, while that of a load-end waveform based on symmetric regular sampling is 3.81%. Thus, the quality of output waveforms based on tangent approximation is superior to that based on symmetric regular sampling, under the same load.

4   Experimental verification

4.1   Software design

According to the overall requirements of the project, a control chip STM32F407ZGT6 was used in this paper, which is a 32-bit ARM Cortex-M4 processor issued by ST. The chip has a clock rate up to 168 MHz, with two advanced control timers. Each timer has three channels, and each channel can output complementary pulses with adjustable dead zones. Besides, on the basis of ARM Cortex-M3,

this chip is extended in terms of digital signal processing (DSP), incorporating a multiply and accumulate (MAC) unit and a single-precision float-point unit (FPU). These functions greatly improve the real-time computation capacity of the control chip, providing software and hardware guarantees for outputting high-precision SPWM pulses and realizing complex industrial control.

A 50 Hz three-phase power-frequency sine wave at a switching frequency of 4.2 kHz is taken as an example. The programming idea based on this control chip is as follows: First, a complementary pulse with a dead zone is output by using a built-in advanced control timer of the chip. Then, a general timer with the same frequency is set to modify pulse width by the cyclic interrupt. Thus, SPWM pulses changing sinusoidally can be output. The advanced control timer TIM1 together with the ordinary timer TIM4 is taken as an example, and specific steps are shown in Fig. 8.

1) The configuration is initialized by the program. First, the multiplexing function of an output pin is configured. TIM1 of the chip STM32F4 has three output channels. Each channel corresponds to a pulse output pin TIM1_CHx and a complementary-pulse output pin TIM1_CHxN, where $x = 1, 2$, and 3. Then, the basic parameters of TIM1 are set. Specifically, the frequency division coefficient PSC and the pulse period Period of TIM1 are set according to switching frequency f_s. The pulse period can

(a) Interrupt program

(b) Main program
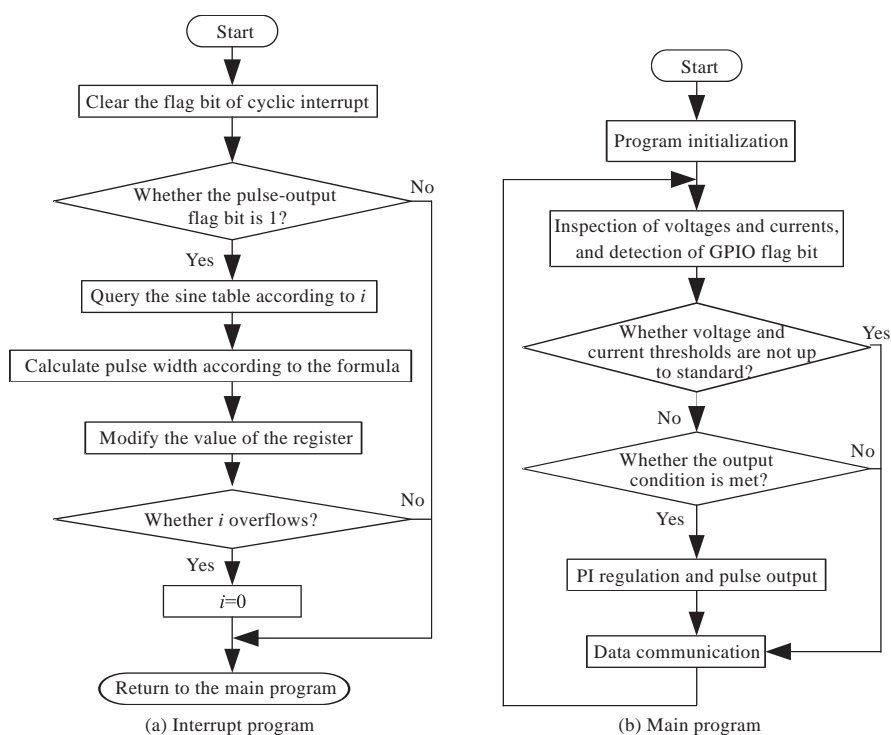
Fig. 8   Flow chart of generation program for SPWM signals

be represented by the count value of the timer.

$$f_s = \frac{f_{CLK}}{PSC \times (Period + 1)} \qquad (10)$$

where $f_{CLK} = 84$ MHz is clock rate.

In order to facilitate subsequent calculation of the sine table and compilation of look-up table statements in the interrupt service function, we set the number of corresponding SPWM pulses in each sine-wave period as N. Then,

$$N = f_s / f_{sin} \qquad (11)$$

where $f_{sin} = 50$ Hz is sine-wave frequency.

TIM1 is set to the PWM output mode to enable complementary output, and the levels of complementary and ordinary channels are set to be of opposite phases. The dead zone of a complementary pulse is set, and the dead time Deadtime is set according to configuration rules of dead-time generators of break and dead-time registers TIM1_BDTR in the STM32F4xx manual. In addition, the ordinary timer TIM4 is initialized to set its frequency to that of TIM1 and its mode to overflow interrupt.

2) The interrupt service function of TIM4 is written and the overflowing interrupt flag bit of TIM4 is cleared every time the interrupt service program is run. At the same time, the pulse width of each pulse in the SPWM pulse sequence is calculated according to Formula (9).

For simplified calculation, a sine-value calculation table (usually an array) with a length of N can be defined in advance. Then, sine values of a sinusoidal period are divided into N parts and stored in the array. As a result, there is no need to calculate the sine values separately in the interrupt service program anymore, and it is only necessary to look up the table according to i. Thus, program crash due to the excessive computation of the interrupt service function can be avoided.

4.2 Verification of high-frequency inverter charging device

According to the simulation model and the software design idea, a high-frequency inverter charging device based on STM32F407ZGT6 was designed in this paper. Its system architecture is shown in Fig. 9, and its key parameters are listed in Table 4. This device consists of an input three-phase power supply, a three-phase rectifier bridge (uncontrolled rectifier bridge), an inverter, an output filter module, a load, a master controller, and a driver. Closed-loop control can be formed by collecting voltages and currents of the DC bus and those at the output end of the inverter.
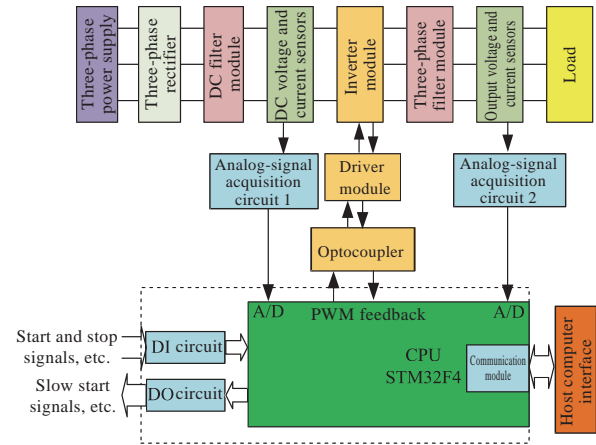
Fig. 9　System architecture of high-frequency inverter charging device

Table 4　Key parameters of the high-frequency inverter charging device

Parameter	Value	Remark
Three-phase input voltage/V	600	Effective line voltage, with a frequency of 300 Hz
DC filter inductance/mH	0.5	—
DC filter capacitance/μF	1 000	—
Output filter inductance/mH	1.5	—
Output filter capacitance/μF	15	Star connection
Output voltage/V	400	Effective line voltage, with a frequenc of 50 Hz
System power/W	6 000	Maximum power
Modulation ratio	—	Modulaiton ratios vary with inputs and outputs
Switching frequency/Hz	4 200	

Infineon's three-phase IGBT inverter module was used, with a withstand voltage of about 1 700 V and a collector current of 300 A in normal operation. Its built-in thermistor can cooperate with the driver module of the inverter bridge to provide more accurate temperatures of the inverter bridge for the master control board. A 6QP0115Txx-Q series IGBT driver board from Bronze Technologies was used as the driver module of the inverter. The driver board can produce drive signals with very short ON-OFF time, and meanwhile has the function of three-phase fault detection and alarming. Before an SPWM control signal generated by the CPU is input into the driver module of the inverter, it should first pass through a high-speed optocoupler isolation chip to isolate external electromagnetic interference and improve the signal's drive capability. Fig. 10 shows a physical diagram of the high-frequency inverter charging device.

(a) Master control board

(b) Appearance of the whole device

Fig. 10　Real device picture of the high-frequency inverter charging device

Without changing the strong-current circuit topology, switching between symmetric regular sampling and tangent approximation can be done by changing the program algorithm. The output waveforms of the three-phase line voltages of the device are shown in Fig. 11. Fig. 11 (a) shows the load-end voltage waveforms obtained by symmetric regular sampling. The effective output three-phase line voltages are 406, 404, and 405 V, respectively, and the frequency is 50 Hz. In view of the precision of actual measurement, output errors are acceptable. From the measurement in a long-time full-load burn-in test, once the test time exceeds 3 h, the inverter will stop due to over-temperature protection of the overheat-triggered device.
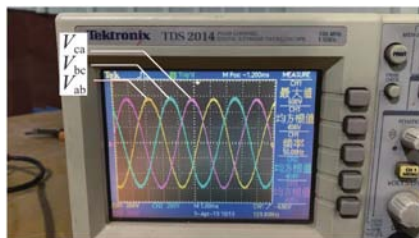
(a) Symmetric regular sampling
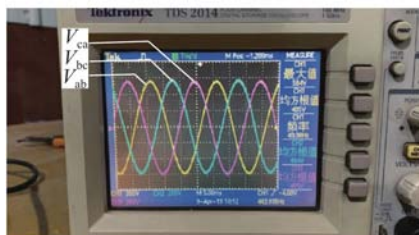
(b) Tangent approximation

Fig. 11　Output waveform of three-phase line voltage

Fig. 11 (b) shows the load-end voltage waveforms obtained based on tangent approximation. The effective output three-phase line voltages are 405, 404, and 405 V, respectively, and the frequency is 49.98 Hz. The output errors are also acceptable. According to the verification by a long-time full-load burn-in test, no over-temperature protection will occur, and the actual working temperature is always in the normal range.

From Fig. 11, the load-end waveforms in the two experiments are almost the same, and only the temperature rises under long-time burn-in testing are different. For further analysis, comparative experiments at different input voltages were carried out in this paper. Table 5 lists the results of FFT analysis.

Table 5　FFT analysis data of comparative experiments

Effective input line voltage/V	THD /%		Actual modulation ratio
	Tangent approximation	Symmetric regular sampling	
480	1.51	3.64	0.95
530	1.45	3.59	0.88
580	1.42	3.57	0.80
630	1.61	3.58	0.74
680	1.93	4.32	0.68

As can be seen from Table 5, the THD of output waveforms in the two experiments is obviously different at different input voltages (that is, different modulation ratios). Specifically, the THD of the output waveforms based on tangent approximation is lower, which means the waveform quality of this method is higher than that of symmetric regular sampling. In Table 5, waveform quality is relatively optimal when the effective input line voltage is 580 V and the modulation ratio is 0.8.

Therefore, according to the verification results of the device, SPWM based on tangent approximation is easy to be implemented. Moreover, it can output high-quality waveforms and perform relatively stably in long-time operations. At present, this method has been applied to a military mobile platform. Verified by the users, it can meet military requirements.

5　Conclusions

In view of deficiencies in traditional sampling methods, as well as practical engineering requirements, SPWM based on tangent approximation was proposed in this paper. Simulation data and experimental results show that this method performs better than symmetric regular sampling in terms of

waveform quality and device stability. Moreover, avoiding deficiencies in traditional asymmetric regular sampling, this method can reduce occupation rates of CPU. This is important for embedded control systems or control systems of single-chip microcomputers.

References

[1] CHEN M X, SHI B, CHEN Y G. A novel sampling method of SPWM Based on DSP [J]. Electrical Automation, 2011, 33 (5): 45−47 (in Chinese).

[2] WANG C Y, HU Q, WANG F L. Implementation of improved asymmetric regular sampling algorithm based on TMS320F28335 [J]. Acoustics and Electronics Engineering, 2017 (3): 25−27, 32 (in Chinese).

[3] ZHOU Y S, GONG H J, ZHANG J, et al. Optimization of sampling methods based on SPWM [J]. Science&Technology Review, 2009, 27 (5): 38−42 (in Chinese).

[4] GAVASKAR R B, MAHESWARI L, GANESWARI K A. Performance improvement of single phase inverter using SPWM [J]. IOP Conference Series: Materials Science and Engineering, 2017, 225 (1): 012071.

[5] MUNOZ R M, VALDERRAMA B H, RIVERA M, et al. An approach to natural sampling using a digital sampling technique for SPWM multilevel inverter modulation [J]. Energies, 2019, 12 (15): 2925.

[6] LI Z Z F, WANG L Z, SHAO X, et al. Simulation implementation of SPWM natural sampling and regular sampling method [J]. Electronic Technology, 2018, 47 (9): 66−68 (in Chinese).

[7] ZHU C B, LI L, WANG X P. Modeling and simulation of voltage and current double loop control based on SPWM inverters [J]. Chinese Journal of Ship Research, 2009, 4 (5): 54−58 (in Chinese).

[8] BAHRAMI A, NARIMANI M. A sinusoidal pulse width modulation (SPWM)technique for capacitor voltage balancing of a nested T-type four-level inverter [J]. IEEE Transactions on Power Electronics, 2019, 34 (2): 1008−1012.

[9] HE L Z, CHENG C. A bridge modular switched-capacitor-based multilevel inverter with optimized SPWM control method and enhanced power-decoupling ability [J]. IEEE Transactions on Industrial Electronics, 2018, 65 (8): 6140−6149.

[10] LI H L, JIANG J G, QIAO S T. Essential relation between three-level SVPWM and SPWM and analysis on output voltage harmonic [J]. Automation of Electric Power Systems, 2015 (12): 130−137 (in Chinese).

[11] GUO Y, SHAO D D, GUO J C, et al. Simulation study of harmonic characteristics of modular multilevel converter in medium voltage DC power system on ship [J]. Chinese Journal of Ship Research, 2019, 14 (1): 134−143 (in Chinese).

[12] WANG T J, RAO X, JIANG X Y, et al. Control strategy study on multi-phase induction motor for one DC amplitude-voltage power system [J]. Chinese Journal of Ship Research, 2011, 6 (6): 75−77, 82 (in Chinese).

基于切线逼近法的非对称规则
采样SPWM 方法

李巍[1], 李维波[*1,2], 徐聪[1], 卢月[1], 陈辉[1]

1 武汉理工大学 自动化学院，湖北 武汉 430070
2 西藏大学 工学院，西藏 拉萨 850012

摘　要：［目的］为改善舰船高频逆变充电装置输出正弦波的质量，同时降低CPU 占用率，提出一种基于切线逼近的非对称规则采样正弦脉冲宽度调制（SPWM）方法。［方法］根据基于切线逼近的非对称规则采样SPWM 方法的基本原理及计算方法，搭建 Matlab/Simulink 仿真模型，设计适用于高频逆变充电装置的软件算法流程，并对切线逼近法的实际输出效果进行仿真对比和实验验证。［结果］仿真结果表明，在纯阻性负载和阻感性负载下，基于切线逼近法的负载端波形的总谐波失真（THD）分别为 2.12% 和 2.08%，其波形质量优于对称规则采样法；实验结果表明，基于切线逼近法的负载端波形的 THD 明显低于对称规则采样法，当输入线电压有效值为 580 V（调制比为 0.8）时，输出波形的质量相对最优。［结论］基于切线逼近的非对称规则采样 SPWM 方法克服了传统对称规则采样法的输出波形质量不高，以及传统非对称规则采样法的采样频率高、CPU 占用率高等缺点，研究成果可为舰船高频逆变充电装置设计提供参考。
关键词：逆变器；正弦脉冲宽度调制（SPWM）；规则采样；切线逼近